THE JOURNAL OF PHYSICAL CHEMISTRY B

Article

pubs.acs.org/JPCB

Impact of Mutations at C-Terminus on Structures and Dynamics of Aβ40 and Aβ42: A Molecular Simulation Study

Nguyen Hoang Linh,[†,‡,▽] Tran Thi Minh Thu,[†,‡,▽] LyAnh Tu,[†,‡] Chin-Kun Hu,[§,∥,⊥] and Mai Suan Li*[,†,#]

[†]Institute for Computational Science and Technology, SBI Building, Quang Trung Software City, Tan Chanh Hiep Ward, District 12, Ho Chi Minh City, Vietnam

[‡]Biomedical Engineering Department, University of Technology - VNU HCM, 268 Ly Thuong Kiet Street, District 10, Ho Chi Minh City, Vietnam

[§]Institute of Physics, Academia Sinica, 128 Academia Road Section 2, Taipei 11529, Taiwan

[∥]National Center for Theoretical Sciences, National Tsing Hua University, 101 Kuang-Fu Road Section 2, Hsinch 30013, Taiwan

[⊥]Business School, University of Shanghai for Science and Technology, 334 Jun Gong Road, Shanghai 200093, China

[#]Institute of Physics Polish Academy of Sciences, Al. Lotnikow 32/46, 02-668 Warsaw, Poland

Supporting Information

ABSTRACT: Alzheimer's disease is presumed to be caused by the formation of intracellular plaques of amyloid β (Aβ) peptides inside neurons. The most abundant Aβ forms are Aβ40 and Aβ42 comprising, respectively, 40 and 42 residues. Recent experiments showed that the triple Gly33Val-Val36Pro-Gly38Val (VPV) mutation causes Aβ42 to become "super-Aβ42" with elevated aggregation rates and toxicity. Upon VPV mutation, oligomerization pathways of Aβ40 become similar to those of the Aβ42 wild type. It was hypothesized that the *super* behavior of Aβ42 occurs due to an enhanced content of the β-turn and β-hairpin, centered at residues 36−37, and the similarity in oligomerization pathways of Aβ40-VPV and Aβ42-WT comes from the increased β-turn population. As this is based on simulation of the truncated fragments, this hypothesis may not be valid for the full-length case, motivating us to perform all-atom molecular dynamics simulations for full-length Aβ sequences. We showed that the results obtained for truncated peptides fall short in explaining the similarity of self-assembly pathways of Aβ40-VPV and Aβ42-WT. Instead, we propose that the similarity is due to not only increased β-turn population but also due to the elevated β-structure of the entire sequence. Similar to VPV, the Gly33Val-Val36Asn-Gly38Leu mutation enhances the β-structure and the C-terminal β-turn making the behavior of Aβ40 similar to that of Aβ42-WT.

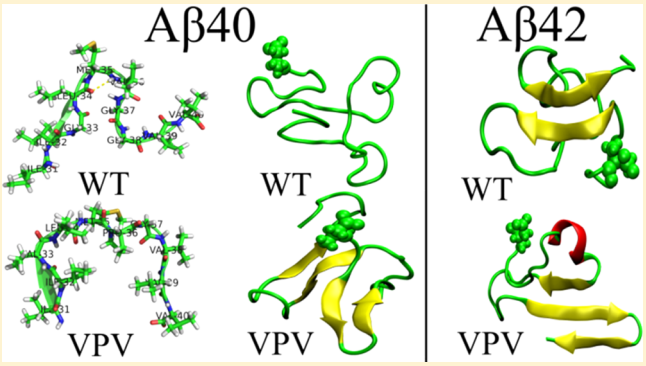

I. INTRODUCTION

Alzheimer's disease (AD) is a chronic neurodegenerative disease that usually starts slowly and worsens over time. The most common symptoms are a difficulty in remembering recent events,[1] problems with language,[2] and visual−spatial search,[3] among other side-effects. There exist three main hypotheses about the AD etiology, involving the tau protein, amyloid cascade, and cholinergic hypotheses.[4,5] However, recent accumulated evidence strongly supports the second hypothesis, which posits that the self-assembly of amyloid β (Aβ) peptides is the main cause of AD.[6,7] As Aβ peptides are proteolytic byproducts of the amyloid precursor protein, one of the strategies to treat AD is to prevent production of Aβ peptides, which are commonly composed of 40 (Aβ40) and 42 (Aβ42) amino acids

In the monomer state, Aβ peptides are mostly a statistical coil (SC) in physiological buffers, but aggregate to form fibrils with a β-sheet structure.[8−11] Aβ42 is the dominant protein component of parenchymal plaques.[12−14] Increasing the amount of Aβ42, or the concentration ratio of Aβ42/Aβ40, is associated with an increased risk of AD.[15,16] In vitro studies showed that Aβ42 displays fibril nucleation and elongation rates that are higher than those of Aβ40,[17] and that Aβ42 forms larger oligomers than does Aβ40.[18−20] Moreover, neither the mature fibrils nor monomers of Aβ peptides are toxic; however, the esthetic of the cerebral defects in AD rather correlates with high levels of oligomers in the brain.[21] This leads to the second strategy to cope with AD that is based on preventing or reversing formation of toxic oligomers,[4] requiring a deep understanding of Aβ structures and self-assembly pathways.

Received: December 22, 2016
Revised: April 15, 2017
Published: April 17, 2017

DOI: 10.1021/acs.jpcb.6b12888
J. Phys. Chem. B 2017, 121, 4341−4354

Aβ40 and Aβ42 oligomerize in different ways: Aβ40 mostly assembles into dimeric, trimeric, and tetrameric species, whereas Aβ42 preferably forms pentamer/hexamer units and then further assembles into larger oligomers such as dodecamers and octadecamers.[22] These behaviors have been confirmed by experiments using ion mobility spectrometry coupled with mass spectrometry.[19] The distinct physical and biological properties of Aβ40 and Aβ42[23−25] are due to their different structures as both peptides are unstructured, but the Aβ42 C-terminus is more rigid than the Aβ40 one.[26−29] The decisive role of the last two hydrophobic amino acids Ile41 and Ala42 in the distinct behaviors of the two peptides was clearly demonstrated.[30] It was shown that the C-terminus of Aβ42 displays resistance to proteolytic digestion.[31]

Recently, using various experimental techniques to study the impact of mutations at the C-terminus on Aβ aggregation, Roychaudhuri et al.[25] made a number of interesting observations. They showed that mutations can alter oligomerization pathways as well as the toxicity of Aβ peptides. In particular, they hypothesized that the triple mutation Gly33Val-Val36Pro-Gly38Val (VPV) generated the so-called "super-Aβ42" by stabilizing the β-turn at Val36-Gly37 and β-hairpin. Thus, the C-terminal turn is the *sine qua non* of Aβ42, and this turn is an attractive target for AD treatment. More importantly, the VPV mutation can convert Aβ40 oligomerization pathways into those of Aβ42 through substantial enhancement of the β-turn at the C-terminus.

One has to stress that Roychaudhuri et al.[25] have interpreted their experimental data based on the assumption that the existence of the β-turn plays a crucial role. However, the β-turn and β-hairpin contents were obtained for truncated fragments $A\beta_{31-40}$ and $A\beta_{31-42}$ and their variants, casting doubt on their interpretation for full-length peptides. In this article, we check their predictions by studying full-length Aβ peptides and mutants using all-atom replica exchange molecular dynamics (REMD) simulations.

We have shown that a β-hairpin structure centered at Val36-Gly37 occurs in the Ile31-Ala42 fragment of Aβ42 variants, but in the Aβ40 case, the Ile31-Ala40 fragment is predominantly a coil. In agreement with the experiments and simulations for truncated peptides,[25] the VPV mutation converts Aβ42 into super-Aβ42 through an enhanced propensity of the β-turn and β-hairpin at the terminal. However, contrary to results obtained from short peptide simulations, this mutation levels up the β-turn population of Aβ40, but not to such an extent that the oligomerization pathways become similar to those of Aβ42 wild type (Aβ42-WT). Thus, the similarity in aggregation pathways of Aβ40-VPV and Aβ42-WT, indirectly obtained from oligomer distributions in the experiment,[25] cannot be explained based solely on increased β-turn propensity at the C-terminal. Instead, we propose that the enhancement of the β-structure of the entire sequence should be taken into account.

We also studied the triple mutation G33V-V36N-G38L (VNL), which increases Aβ hydrophobicity but to a lesser extent compared to that increased by VPV. We predict that, similar to VPV, VNL can make Aβ40 oligomerize in the same way as Aβ42-WT through enhanced β-structure and β-turn content at the C-terminus. In addition, upon VNL mutation, the β-hairpin becomes more populated leading to super-Aβ42 behavior.

II. MATERIALS AND METHODS

II.I. Initial Structures of Aβ Peptides and Mutants. The WT structures of the Aβ40 and Aβ42 peptides were taken from the Protein Data Bank (PDB)[32] with the PDB codes 1BA4 and 1Z0Q, respectively. These structures were obtained in a water−micelle environment, but the choice of initial conformations for REMD simulation is not important. The structures of the mutants with substitutions Gly33Val, Val36Pro, Gly38Val (VPV); Gly33Val, Val36Asn, Gly38Leu (VNL); Gly33Val, Val36Asp, Gly38Leu (VDL), and V36D were obtained from the original structures using the RaptorX website server.

II.II. Molecular Dynamics Simulations. Simulations were performed with the OPLS-AA/L force field[32] for protein and the Generalized Born (GB) model[33] for implicit solvent using GROMACS software version 4.5.5.[34] The OPLS-AA force field was used in this work because it generated conformations for the Aβ42 monomer that match the structure of the Aβ peptide obtained by the NMR data.[26] Moreover, previous studies demonstrated that this force field is suitable for simulation of aggregation of several Aβ fragments.[35,36] We chose the GB implicit solvent not only because of the limitation of our resource, but also because prior studies showed that the GB model gives reasonable results for Aβ variants[24,37] and other systems.[38,39] One of the limitations of the implicit solvent is that it ignores interactions with water. Therefore, the success of the GB approximation in studying Aβ thermodynamics is presumably due to the fact that water bridges do not contribute significantly to the stability of highly flexible molecules such as intrinsically disordered Aβ.[29]

We simulated WT and mutants of Aβ peptides in the same conditions. The leapfrog algorithm[40] was employed to integrate the equations of motion with a time step of 2 fs. The length of all bonds was constrained by the LINCS algorithm.[41] V-rescale temperature coupling was used to change the velocity of atoms periodically but keep the temperature of the system stable,[42] with a relaxation time of 0.1 ps. The nonbonded interactions were calculated with an infinity cutoff.

Twelve replicas were used for REMD simulation for all systems. The temperatures of the replicas were chosen by the method of Partrisson and van der Spoel.[43] The range of temperatures were from 290.16 to 490.16 K for all systems (T = 290.16, 300, 311.80, 326.18, 343.14, 361.92, 380.83, 400.69, 421.86, 444.02, 466.14, 490.16 K). Each replica was exchanged every 2 ps, which is large enough compared to the coupling time to the heat bath. Each replica was run for 1000 ns, and production data were collected every 10 ps.

II.III. Tools and Measures Used for Data Analysis. *II.III.I. Secondary Structure.* The STRIDE algorithm[44,45] was used to calculate the secondary structures of the Aβ peptides. The advantages of this algorithm is that the definition is based not only on information of dihedral angles, but also on the hydrogen bonds (HBs) of protein.

II.III.II. Salt Bridge (SB). An SB between two charged residues may have an impact on the structure of the β-sheet. If the distance between two specific atoms remains within 4.6 Å, an SB was formed. In this work, we consider the distance between the Cγ atom of Asp23 residue and the Nζ atom of Lys28 residue.

II.III.III. Free-Energy Landscapes. We calculated the free-energy surface (FES) of the systems by $G(V) = -k_BT[\ln P(V) - \ln P_{max}]$, where $P(V)$ is the probability distribution obtained from the MD simulation results. P_{max} is the maximum of the

DOI: 10.1021/acs.jpcb.6b12888
J. Phys. Chem. B 2017, 121, 4341−4354

distribution, which is correlated to $\Delta G = 0$ for the lowest-free-energy minimum. Dihedral principal component analysis (dPCA)[46] and the two most important eigenvalues $V1$ and $V2$ were used to construct the FES.

II.III.IV. Contact Map. To construct side-chain contact maps, we calculated the distance between the centers of masses of two residues. If this distance is within 6.5 Å, then the corresponding contact is formed.

II.III.V. β-Turn and β-Hairpin. The β-turn occurs on four consecutive residues from i to $i + 4$ and is classified into nine types based on the dihedral angles of $\varphi(i + 1)$, $\psi(i + 1)$, $\varphi(i + 2)$, and $\psi(i + 2)$.[47] The residues that make up a β-turn are typically amino acids with strong turn-forming propensity that allows the polypeptide backbone to adopt a conformation where the $C\alpha(i) - C\alpha(i + 3)$ distance is less than 7.0 Å. Each type of β-turn has its own mean dihedral angle, but only type I′ and II″ are found predominantly in a β-hairpin.[48,49] A β-hairpin is formed by a turn connecting two β-strands in antiparallel directions by loops of various lengths. A loop can be classified into different types according to the number of residues in the loop region and residues closing the loop.

III. RESULTS AND DISCUSSION

We chose $T = 311.8$ K, which is closest to the physiological temperature $T = 37$ °C, for data analysis.

III.I. Equilibration Procedure. The total simulation time was 1000 ns for all studied peptides and variants. To obtain the equilibration time t_{eq}, we plotted the $C\alpha$ root-mean-square displacement (RMSD) as a function of time (Figures 1 and 2). Obviously, $t_{eq} \approx 210$ ns, because after this time, the RMSD of all systems becomes stable, fluctuating around its equilibrium value. To make sure that the data were well equilibrated we adopted the following procedure. Suppose we carry out one MD run with a duration of t_1 and another one which is 2-fold longer than the first run, $t_2 = 2t_1$. If the thermodynamic quantities computed at equilibrium for two MD runs match then the system can be considered as well equilibrated. Because $t_2 = t_{full} = 1000$ ns, we have $t_1 = 500$ ns. The secondary structures were calculated in two time windows $[t_{eq}, t_1]$ and $[t_{eq}, t_{full}]$ or [210, 500 ns] and [210, 1000 ns]. Skipping the first 210 ns spent on equilibration, we obtained the β-content at $T = 311.8$ K for all sequences, as shown in Figures 1 and 2. Within error bars, the β-contents obtained in the two time windows are the same. This also holds for helix, turn, and coil (results not shown), implying that REMD simulations afford the equilibrated data for all studied systems. In what follows, we will present the results obtained in the [210, 100 ns] window. The data convergence was important because it showed that our sampling is sufficient to produce a representative subset of the whole space and, therefore, reliable results.

III.II. Secondary Structures of Aβ40 and Its Variants: upon VPV and VNL Mutation, Self-Assembly Pathways of Aβ40 Are Expected To Be Similar to Those of Aβ42. Using STRIDE software at equilibrium and $T = 311.8$ K, we obtained the mean secondary structures of Aβ40 as 11.97, 3.89, 65.69, and 18.45% for β, helix, turn, and coil, respectively (Table 1). Low β (11.97%) and helix (3.89%), and high SC (84, 14% for turn + coil) match with experimental results reported by Zhang et al.[50] and Danielsson et al.[51] showing that the Alzheimer's Aβ peptide adopts as an SC in the water environment. Using filtration through a 10 000 molecular weight cutoff and circular dichroism of low molecular weight Aβ40 aggregates, 88% of random coil and turn, 12% of β-strand, and 0% of α-helix were obtained in an environment of pH 7.5, $T = 295$ K at day 0.[52] These data are in line with ours. In contrast, Ono et al. showed that Aβ40 monomer has a 25% β-content,[53] which is twice as high as our value. The α-content of 3.89% is lower than that obtained previously by coarse-grained UNRES[54] but higher than that of the all-atom results of Viet et al.,[23] Truong et al.,[24] and Sgourakis et al.,[26] who used Amber-derived PARM94, PARM96, MOD-PARM, GROMOS, and OPLS force fields and a recently improved version of the Amber force field PARM99SB employed by Yang and Teplow.[29] Our estimate of β-content (11.97%) is a bit higher than the results reported by these groups. Using REMD with the OPLS-AA/L force field and the TIP3P water model, Rosenman et al. reported $\beta \approx 25\%$, which seems to be high for Aβ40.[55] The discrete molecular dynamics combined with the four-bead protein model in implicit solvent gives $\beta \approx 19\%$ for Aβ40 and 15% for the truncated $A\beta_{3-40}$,[56] which are higher values than ours.

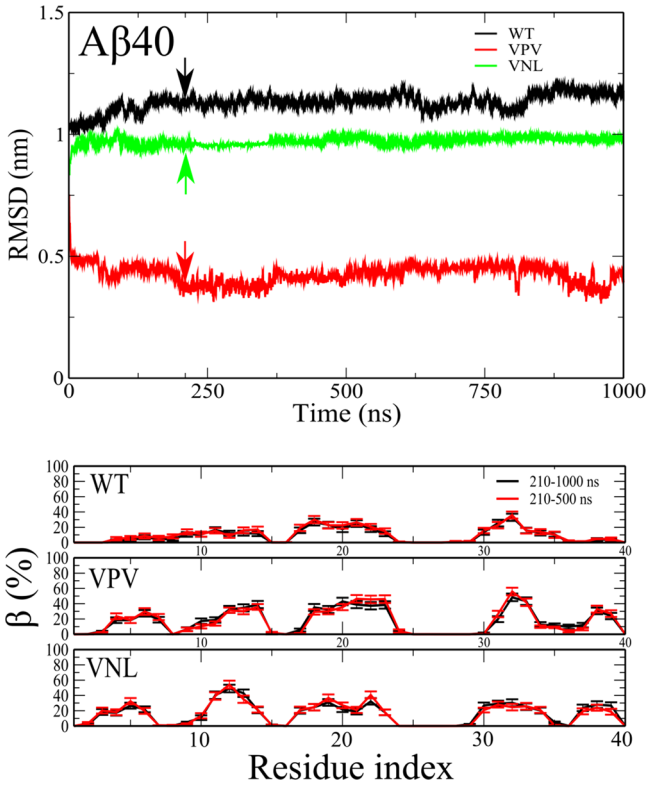

Figure 1. Upper part) Time dependence of $C\alpha$-RMSD at $T = 311.8$ K for five Aβ40 sequences. Arrow refers to the equilibration time t_{eq} = 210 ns when RMSD saturates. (Lower part) The β-content, obtained for two time windows at $T = 311.8$ K for five Aβ40 sequences. Black and red refer to window [210−1000 ns] and [210−500 ns], respectively. Error bars come from averaging over snapshots collected at equilibrium.

Upon mutation, the total β-propensity of Aβ40 leveled up from 11.97 to 16.81%, and 17.08 and 17.28% in VNL and VPV, respectively (Table 1). Although these mutations are distinct, the difference in β-structure is insignificant. Within error bars, the β-content of VPV (17.08 ± 2.5%) is the same as that of Aβ42-WT (21.95 ± 1.91%,Table 2). Because the propensity to self-assembly is controlled by the population of the fibril-prone state of the monomer[57] or by the β-content of the Aβ peptides, this result is in accord with experiments[25] that showed that VPV makes Aβ40 aggregate in the same manner as Aβ42. It

DOI: 10.1021/acs.jpcb.6b12888
J. Phys. Chem. B 2017, 121, 4341−4354

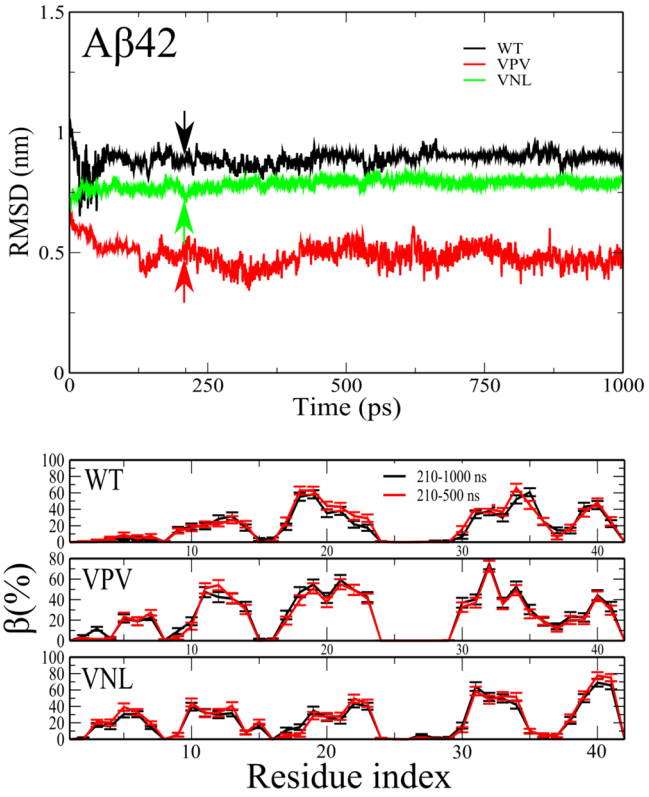

Figure 2. (Upper part) Time dependence of Cα-RMSD at T = 311.8 K for five Aβ42 sequences. Arrow refers to the equilibration time t_{eq} = 210 ns when RMSD saturates. (Lower part) The β-content, obtained for two time windows at T = 311.8 K for five Aβ42 sequences. Black and red refer to window [210−1000 ns] and [210−500 ns], respectively. Error bars come from averaging over snapshots collected at equilibrium.

Table 1. Average Secondary Structures of Aβ40 and Its Mutants[a]

	Aβ40		
content (%)	WT	VNL	VPV
β	11.97 ± 1.44	16.81 ± 2.23	17.08 ± 2.50
α	3.89 ± 1.23	1.75 ± 1.27	1.53 ± 0.53
turn	65.69 ± 9.72	59.17 ± 8.30	59.70 ± 7.88
coil	18.45 ± 3.54	22.27 ± 4.06	21.69 ± 3.66

[a]Results were obtained at equilibrium and 311.8 K.

Table 2. Average Secondary Structures of Aβ42 and Its Mutants[a]

	Aβ42		
content (%)	WT	VNL	VPV
β	21.95 ± 1.91	22.1 ± 3.13	24.40 ± 3.19
α	2.09 ± 1.70	4.07 ± 3.00	2.53 ± 1.46
turn	60.01 ± 7.72	56.73 ± 6.95	54.74 ± 6.45
coil	15.95 ± 3.23	17.11 ± 3.14	18.33 ± 3.25

[a]Results were obtained at equilibrium and 311.8 K.

should be noted that Roychaudhuri et al.[25] interpreted their experimental data on the similarity of the oligomerization pathways of Aβ42-WT and Aβ40-VPV as a consequence of enhanced content of β-turn centered at residues 36 and 37 at the C-terminus. However, their interpretation was based on simulation results obtained for truncated fragments and as discussed in detail below, this is not valid for the full-length case. Here, we propose a different scenario whereby in addition to β-turn, one has to take into account the overall β-structure or the propensity of the fibril-prone conformation N* in the monomer state.

In the VPV mutation, the β-content increases significantly at residues 5−7, 11−14, 19−23, 32−33, and 37−40. This per-residue distribution mimics the distribution of Aβ42-WT, where the β-content levels up at 11−14, 18−21, 31−35, and 38−41 (Figure 4). In the case of Aβ40-VNL, the β-structure of 3, 10−14, 33−40 residues is higher than the WT (Figure 3). Together with VPV, this variant has the same trend whereby the β-content increases at the C-terminus making it more rigid than the N-end, as observed in Aβ42-WT. In addition, as is evident from Tables 1 and 2, within error bars, Aβ40-VNL and Aβ42-WT have the same β-contents. Thus, we predict that the VNL mutation also converts the Aβ40 behavior to Aβ42 behavior, as was observed experimentally in the VPV case.[25] The VNL mutation has a minor effect not only on the overall content of α-helix, turn, and coil but also on their per-residue propensities (Table 1 and Figure 3).

III.III. Secondary Structures of Aβ42 and Its Mutants: Mutation-Induced Super-Aβ42? As is evident from Tables 1 and 2, the β-content of Aβ42 (21.95%) is approximately 2-fold higher than that of Aβ40 (11.97%), which is consistent with the results reported in prior theoretical works[26,29,58,59] and experimental observation[60] whereby Aβ42 aggregates much faster than Aβ40, having a higher population of N* state. The high β-content occurs at residues 17−23 (Figure 4) in the central hydrophobic region, in line with Rosenman et al.[55] who observed the elevated β-population at residues 16−23 using the OPLS-AA/L force field with explicit water model TIP3P. Ball et al. showed that the β-structure is rich at residues 16−21, having employed the Amber ff99SB force field and TIP4P-Ew water model.[61] Besides the central hydrophobic region, the β-content is enhanced at the C-terminal at residues 31−35 and 39−41 (Figure 4), whereas other theoretical studies showed that the β-structure is mainly populated in the 38−41,[26] 32−36,[29] 27−37,[55] 29−36,[61] or 37−40[62] regions. The C-terminal is much more ordered than the N-terminal, which is consistent with the fact that the C-terminal is fibril-prone, as observed in the experiments of Luhrs et al.[10] and in simulations where Aβ42 fibril growth initiates from this terminal.[63] In contrast to our study, other theoretical works showed that the C-terminal is poorer in β-structure than the N-terminal.[58,64] The β-content obtained in our simulation is higher than that of Velez-Vega and Escobedo,[65] Yang and Teplow,[29] and Cote et al.,[66] but significantly lower than the result reported by Mitternacht et al.[68] Such an abundance of β-structure, obtained by these authors, may be associated with omission of the electrostatic interaction in their force field.[66]

Similar to Aβ40, the α-content of Aβ42 is considerably lower than that of β, turn, and coil (Table 2), which is in accord with reports from other groups,[64,65,67] but it is lower than that reported by Yang and Teplow.[29] At equilibrium, the random coil (coil + turn) is 76%, implying that Aβ42 is more structured than Aβ40, which has a random coil of 84%. Our result falls into the range of other theoretical estimates[26,29,64,65] but is still lower than that of Mitternacht et al.[68]

Upon mutation, the β-content increases slightly from 21.9 to 24.40 and 22.10%, respectively, for VPV and VNL (Table 2), implying that the difference between mutations is minor. Because Aβ42-WT is already a β-rich structure, the impact of

DOI: 10.1021/acs.jpcb.6b12888
J. Phys. Chem. B 2017, 121, 4341−4354

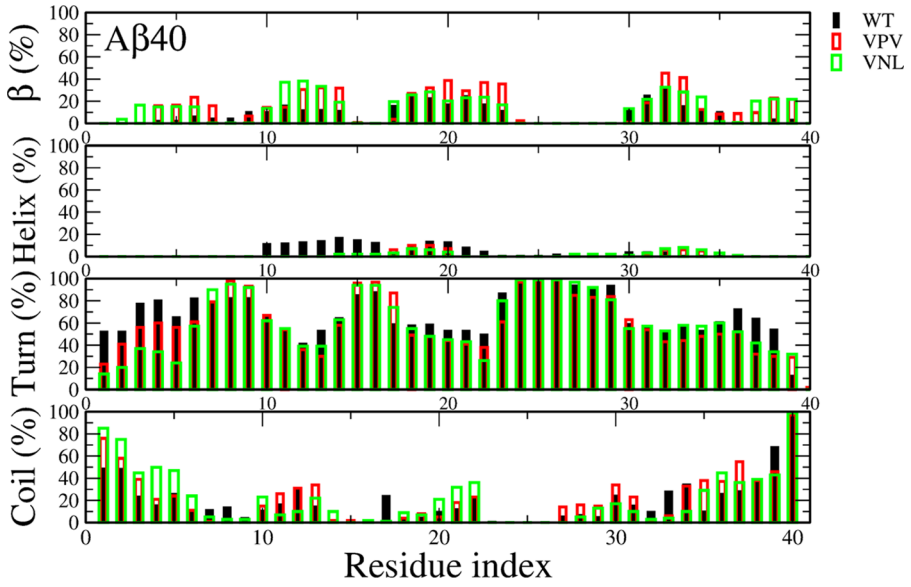

Figure 3. Per-residue distributions of secondary structures of Aβ40 and its mutants. Results were obtained at equilibrium and 311.8 K.

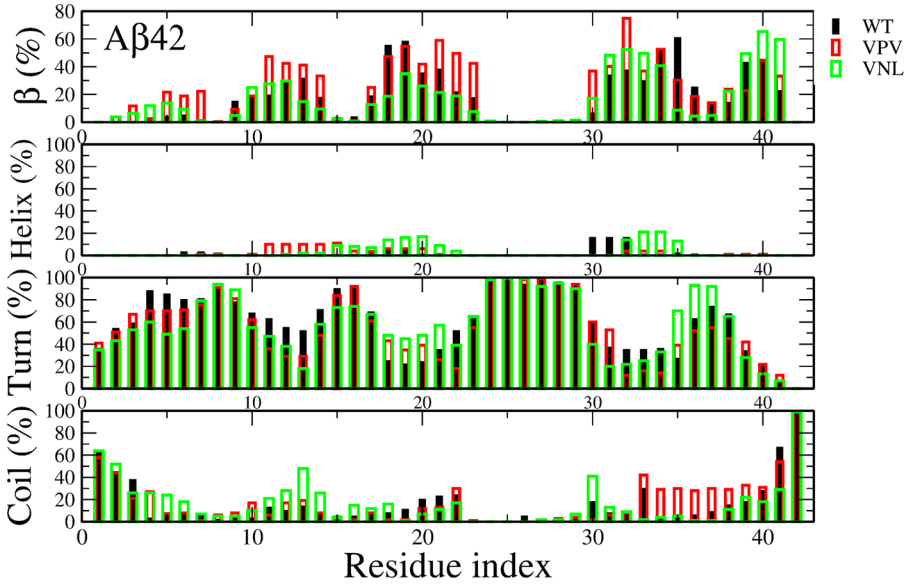

Figure 4. Per-residue distribution of secondary structures of Aβ42 and its mutants. Results were obtained at equilibrium and 311.8 K.

these mutations is not as strong as in the Aβ40 case. Among the two mutants, VPV has the higher β-content, but within error bars all variants including WT have the same β-propensities. Therefore, based on the β-structure populations, we are not able to explain the super behavior of Aβ42 upon VPV mutation.[25] As shown below, this experimental observation may be understood based on the substantial increase of populations of β-turn and β-hairpin at the C-terminus.

For VPV, the β-structure increases dramatically in the 3−7, 11−14, 20−23, and 30−41 regions, whereas VNL reduces β-content at residues 17−23 but promotes it at the C-terminal (Figure 4). Overall, the variants with triple mutations have a minor helix structure, but the α-propensity levels up from 2.09% in WT to 2.53 and 4.07 in VPV and VNL, respectively. The helix content increases in the N-terminus, 10−20, and 30−35 regions. Mutations VPV and VNL slightly reduce the SC (turn + coil) from 75.96% of WT to 73.84 and 73.07%, respectively, for VNL and VPV (Table 2).

III.IV. FESs. Figures 5 and 6 show representative structures on the FESs of the VPV and VNL mutations. Overall, the C-terminus of the Aβ42 variant is more ordered than that of Aβ40-WT.

The FES of Aβ40 has six most populated conformations (Figure 5), whereas the VPV mutation FES, which is narrower in $V1$ and broader in $V2$, has seven basins. Table 3 gives the population of the free-energy local minima and the secondary structure compositions. In Aβ40-WT, S5 and S6 are more ordered than the other states having β-content $\approx$ 30 and 20%, respectively. S5 and S6 are compatible with the most dominant structures obtained by Ball et al.[61] and Rosenman et al.[55] The α-structure does not occur in any of the structures except S3, which has α = 15% with 16.4% population, whereas the turn and coil are present everywhere. The dominant structures in Figure 5 correctly describe the main feature that VPV and VNL enhance the β-structure of Aβ40. In the VPV mutation, the β-structure appears in almost all conformations and the two most

DOI: 10.1021/acs.jpcb.6b12888
J. Phys. Chem. B 2017, 121, 4341−4354

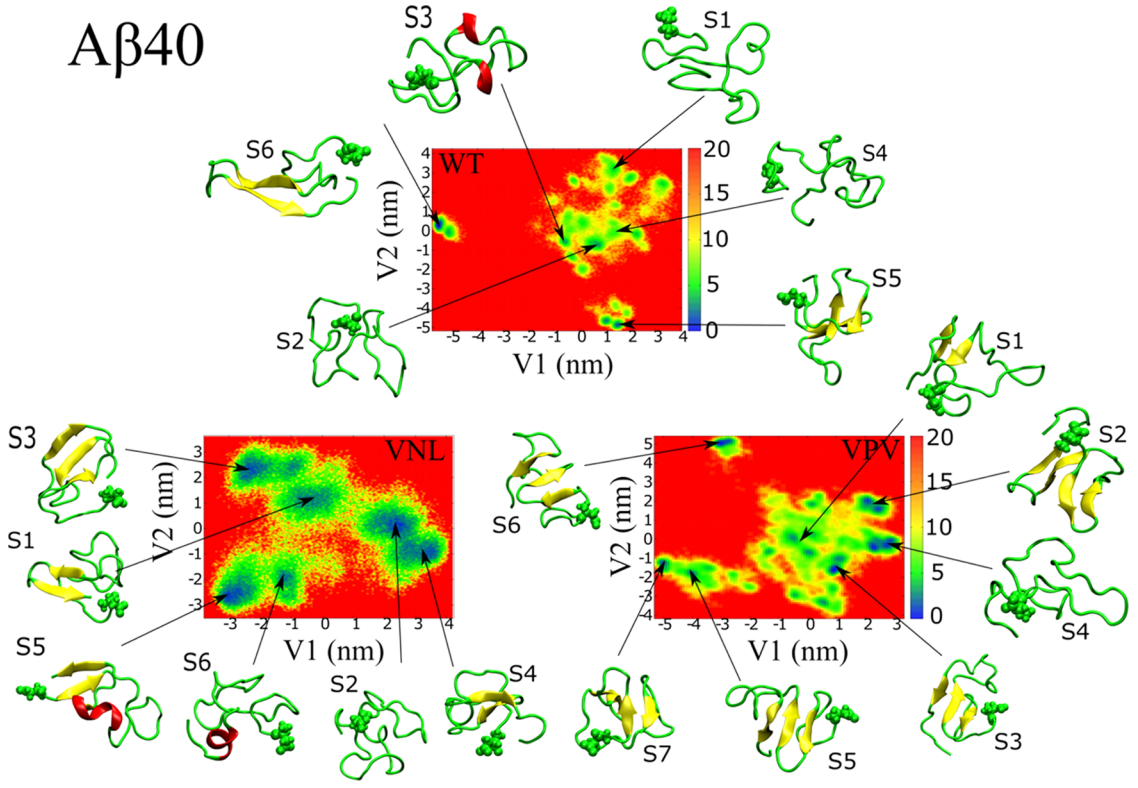

Figure 5. Free-energy landscape of Aβ40 and its mutants as a function of the first two principal components *V*1 and *V*2. The results were obtained from the dPCA analysis at 311.8 K. The first residue is highlighted using its all-atom structure.

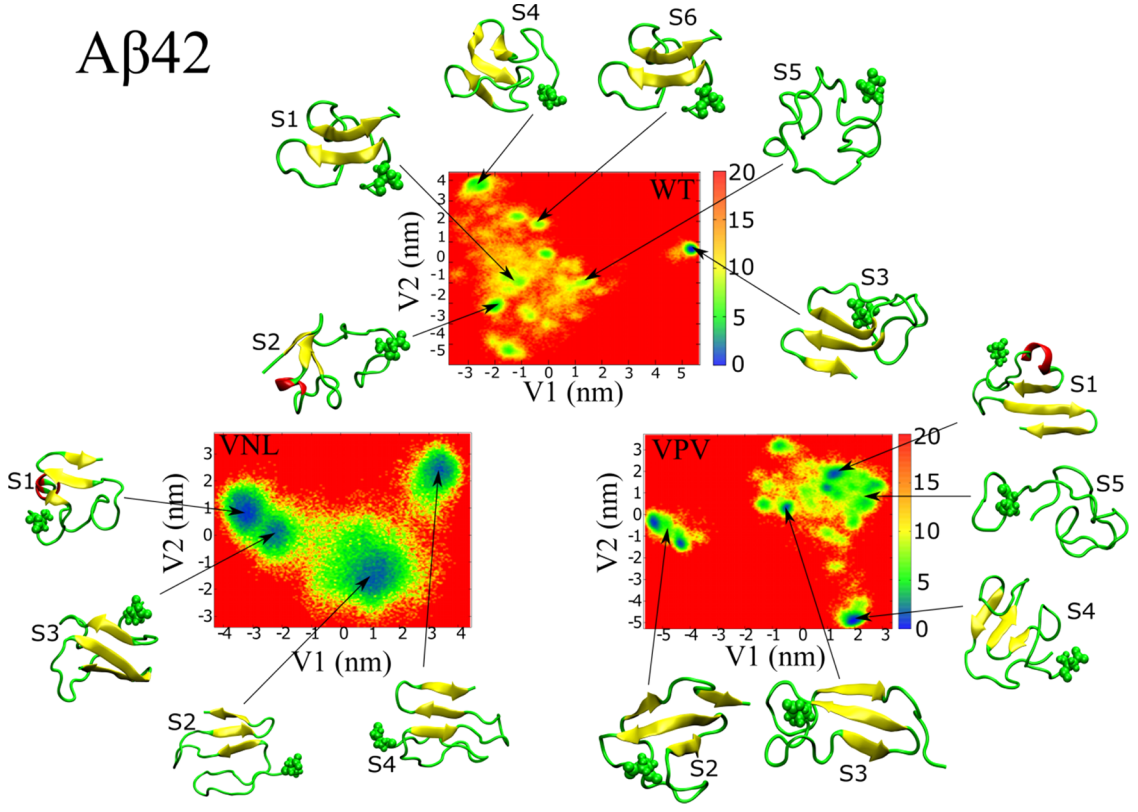

Figure 6. Free-energy landscape of Aβ42 and its mutants as a function of the first two principal components *V*1 and *V*2. The results were obtained from the dPCA analysis at 311.8 K. The first residue is highlighted using its all-atom structure.

populated, S1 and S2, have 10 and 32.5% β, respectively. S4 with 15.3% population has neither β- nor α-structure (Table 3). For Aβ40-VNL, S2 is in the SC and a short helix appears in S6, whereas the rest of the conformations have a β-structure

DOI: 10.1021/acs.jpcb.6b12888
J. Phys. Chem. B 2017, 121, 4341−4354

Table 3. Characterization of the Conformational States (S) of the WT and Mutations of Aβ40 on the Free-Energy Landscapes Shown in Figure 5

system	S	P	β	α	turn	coil
Aβ40-WT	1	22.7	0.0	0.0	65.0	35.0
	2	17.9	0.0	0.0	58.8	41.2
	3	16.4	0.0	15.0	70.0	15.0
	4	14.2	0.0	0.0	77.5	22.5
	5	12.6	30.0	0.0	45.0	25.0
	6	11.6	20.0	0.0	55.0	25.0
Aβ40-VPV	1	27.1	10	0	50	40
	2	19.3	32.5	0	30	37.5
	3	15.5	22.5	0	65	12.5
	4	15.3	0	0	65	35
	5	8.4	22.5	0	65	17.5
	6	7.7	20	0	57.5	22.5
	7	6.6	25	0	50	25
Aβ40-VNL	1	19.5	15	0	50	25
	2	18.4	0	0	77.5	22.5
	3	18.0	27.5	0	45.0	27.5
	4	17.0	15	0	67.5	17.5
	5	15.2	25	15	37.5	22.5
	6	11.8	0	12.5	45.0	37.5

ranging from 15 to 27.5% (Table 3). The C-terminus structures of the most populated conformers for Aβ40 and its mutants are in SC (Figure 7), and more importantly, we do not observe a β-turn, which may play a crucial role in oligomerization and toxicity.[25] Only one, zero, and three HBs appear in WT, VPV, and VNL, respectively.

In Aβ42-WT, apart from the low populated S5 (11.6%), the dominant structures contain β-strands (Figure 6), which is consistent with the result of Ball et al.[61] who showed that β-strands occur in all representative conformations. However, Rosenman et al. reported that only the most important structure with a population of 46% has two β-strands.[55] Note that S3 and S4 in our simulations even have three short β-strands (Figure 6). The sharp difference between Aβ40 and Aβ42 is that only the 12.6% populated S5 of Aβ40 has β-structure (30%), whereas in Aβ42, all conformations contain the β-structure, except S5 with 11.6% of population (Table 4). The β-content slightly increases upon the mutations VPV and VNL (Table 2) and the FESs (Figure 6) display the same trend that almost all dominant structures of the mutants are populated with the β-structure.

Figure 7 shows the structures at the C-terminal of the most populated conformers for Aβ42 and its mutants. Although the Aβ42 C-terminus appears to be overall disordered, its most populated structure (19%) has a β-hairpin with the turn located at residues 36 and 37. The C-terminus of VNL and VPV also has a β-hairpin. This observation matches the experimental result of Roychaudhuri et al.,[25] whereby the most populated conformers of Aβ42 and Aβ42-VPV have their C-terminus structure as a β-hairpin. For the most populated structures, the VPV mutant has a β-content three-fold higher than that of the

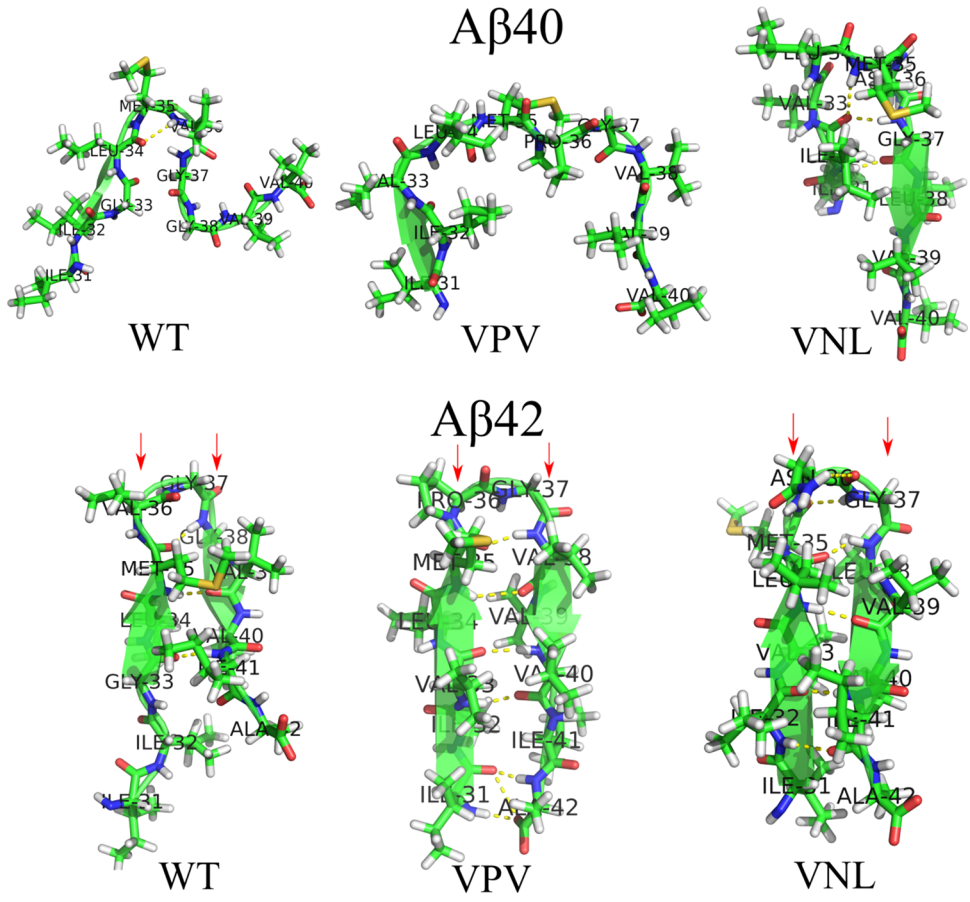

Figure 7. Structures of the most populated conformers for each peptide at the C-terminal of Aβ40 and Aβ42 and their mutants. In the Aβ40 case 1, 0, and 3 HBs occur, respectively, in WT, VPV, and VNL, whereas for Aβ42 there are 3, 7, and 5 HBs in WT, VPV, and VNL.

DOI: 10.1021/acs.jpcb.6b12888
J. Phys. Chem. B 2017, 121, 4341−4354

Table 4. Characterization of the Conformational States (S) of the WT and Mutations of Aβ42 on the FESs Shown in Figure 6

system	S	P	β	α	turn	coil
Aβ42-WT	1	19.0	19.0	7.1	59.5	14.4
	2	18.5	14.3	0.0	73.8	11.9
	3	17.1	23.8	0.0	57.2	19.0
	4	14.8	23.8	0.0	54.8	21.4
	5	11.6	0.0	0.0	75.0	25.0
	6	9.7	23.8	0.0	71.4	4.8
Aβ42-VPV	1	24.6	33.3	11.9	47.6	7.1
	2	20.6	35.7	0.0	47.6	16.7
	3	16.2	28.6	0.0	50.0	16.7
	4	16.0	19.0	0.0	52.4	28.6
	5	15.9	0.0	0.0	61.9	23.8
Aβ42-VNL	1	44.7	16.7	11.9	69.0	2.4
	2	22.1	21.4	0.0	26.2	31.0
	3	16.8	31.0	0.0	57.1	9.5
	4	16.3	21.4	0.0	47.6	7.1

WT, which is consistent with the experimental result whereby VPV displayed a high β-content immediately after dissolution, whereas Aβ42-WT existed in SC form after 5 days of incubation.[25]

In VPV, the β-hairpin is stabilized by seven HBs (Figure 7) and hydrophobic interactions between Ile31-Ala42, Ile32-Ile41, Val32-Val40, Leu32-Val39, and Met35-Val38. The hairpin in the WT is less stable than that of VPV as only three HBs contribute to its stability (Figure 7). The hairpin at the C-terminus of Aβ42-VNL is maintained by five HBs and hydrophobic interactions between the same pairs of residues as in the VPV case.

III.V. Asp23-Lys28 SB. *III.V.I. Definition of SB Based on the Distance between Atoms C^{γ}_{23} and N^{ζ}_{28}.* Because SB Asp23-Lys28 plays an important role in the formation of the cross-β structures of fibrils,[69] we studied it in detail. The distributions of the distances between atoms C^{γ}_{23} and N^{ζ}_{28} of Aβ40-WT and Aβ42-WT have one and two peaks, respectively (Figure 8), implying that the SB of the latter is less flexible. This result is also supported by data on the mean SB distance, which is shorter for Aβ42 (7.97 Å) than for Aβ40 (8.59 Å). Because imposing a constraint on the Asp23-Lys28 SB enhances fibril formation,[69] our observation agrees with the well-known fact that Aβ42 self-assembles faster than Aβ40.

Upon VPV and VNL mutation the SB flexibility of Aβ40 does not change as the mean distance between C^{γ}_{23} and N^{ζ}_{28} remains nearly the same (≈8.7 Å) (Figure 8). Therefore, the change in aggregation rates is rather due to enhanced β-content than due to reduced SB flexibility. The situation is different for the Aβ42 case, where VPV and VNL increase the SB distance from 7.9 ± 2.4 for WT to 9.4 ± 1.7 and 9.0 ± 2.5 Å (Figure 8) suggesting a slowing down of self-assembly. However, one can expect that this effect is not strong because, within error bars, the mean distances of the three variants are the same.

Assuming that SB is formed provided the C^{γ}_{23}–N^{ζ}_{28} distance is less than 4.6 Å, we showed that the population of SB in Aβ42 is highest but remains low (1.77%) (Table S1). Although the population of Aβ42 is poor, this result is in qualitative agreement with the experimental fact that due to reduced flexibility of the Asp23-Lys28 SB Aβ42 is more fibril-prone than Aβ40.

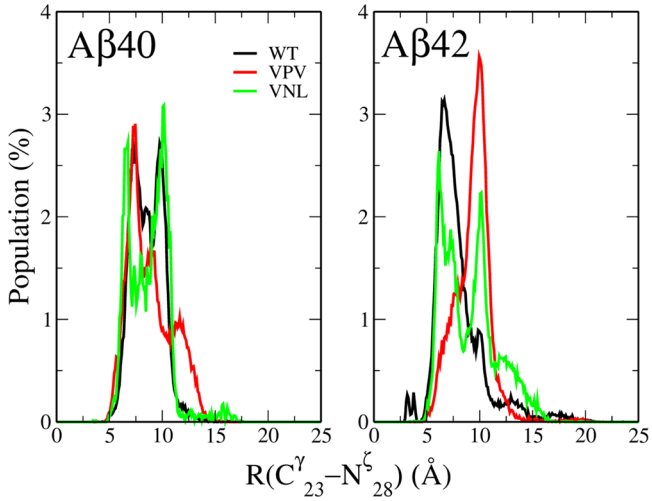

Figure 8. Distribution of Cα23–Cα28 distances of SBs of Aβ and their mutants. In the Aβ40 case, the mean distances are 8.6 ± 1.5, 8.9 ± 2.1, and 8.8 ± 1.9 Å for WT, VPV, and VNL, respectively. For Aβ42, the distances are 7.9 ± 2.4, 9.4 ± 1.7, and 9.0 ± 2.5 for WT, VPV, and VNL, respectively.

III.V.II. More Rigorous Definitions of SB. Because the definition of SB based on the distance between atoms C^{γ}_{23} and N^{ζ}_{28} is flexible, we may have overestimated the SB population. To check this, we applied a more rigorous definition based on HB formation, which is equivalent to SB formation.

Note that the HB between residues 23 and 28 may be formed by the donor atom N^{ζ}_{28} bound to the H atom and acceptor atom O^{δ}_{23} of Asp23. We used the standard criterion that HB occurs if the distance between donor and acceptor atoms is within 3.5 Å, and the acceptor–hydrogen-donor angle is ≤135° (Section II). Using this criterion and snapshots collected in equilibrium, one can show that the populations of Asp23-Lys28 SB of all variants (Table S2) remain practically the same as in the case when the definition is based on the C^{γ}_{23}–N^{ζ}_{28} distance (Table S1). Thus, the SB definition based on the HB does not change the results obtained by using the distance between atoms C^{γ}_{23} and N^{ζ}_{28} to measure the SB lifetime.

Next, we consider the SB adopting the definition from Kumar and Nussinov's paper[70] whereby a SB is formed if (1) the centroids of the side-chain charged groups of Asp23 and Lys28 lie within 4.0 Å of each other and (2) at least one pair of Asp or Glu side-chain carboxyl oxygen atoms and side-chain nitrogen atoms of Arg, Lys, or His are within a 4.0 Å distance. With this definition we obtained the SB populations for all sequences (Figure S3) showing that the three definitions provide the same result for the SB lifetime during MD simulation.

III.VI. SB Contact Map. Figure 9 shows the contact maps of all 18 SBs formed by three positively and six negatively charged residues for the six variants. The Lys28-Asp23 SB population of Aβ42-WT (68.2%) is higher than that of Aβ40-WT (50.6%). For the Aβ40 case, both mutations VPV and VNL slightly reduce this population. For Aβ42, VPV levels up the propensity of Lys28-Asp23 contact to 75.5%, but VNL reduces it to 66.5%. Nevertheless, all Aβ42 variants have a less flexible SB compared to those of the Aβ40 sequences as Aβ40-VPV and Aβ40-VNL are populated for 47.7 and 40% of simulation time, respectively. The population of the Lys28-Glu22 SB of Aβ40-VPV is 22.3%,

DOI: 10.1021/acs.jpcb.6b12888
J. Phys. Chem. B 2017, 121, 4341–4354

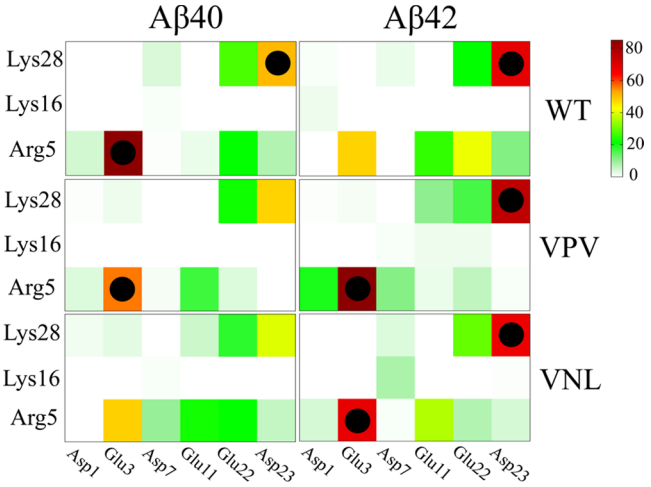

Figure 9. SB contact maps obtained at equilibrium at T = 311.8 K using the definition of side-chain contact described in Section II. Black circles refer to contacts that have a population exceeding 50%.

which is very close to the 21.4% of Aβ42-WT, which is consistent with the experimental finding that[25] the VPV mutation causes Aβ40 to oligomerize similarly to Aβ42-WT. This observation is also supported by the almost equal populations of the Arg5-Glu11 contact of Aβ42-WT and Aβ40-VPV (Figure 9). The difference between the two contacts maps is that the Arg5-Glu22 and Arg5-Asp23 SBs of Aβ42-WT are more populated than those of Aβ40-VPV. However, because their propensities are well below 50%, this discrepancy, presumably, does not result much in a difference in their behaviors.

The propensity of the Arg5-Glu11 and Arg5-Glu22 SBs of Aβ42-WT is higher than that of Aβ40-WT. VNL does not preserve this trend because Aβ42-VNL has a 7.4 and 4.1% population for Arg-Glu11 and Arg5-Glu22 against the 21.3 and 5.8% populations of Aβ40-VNL. Due to proximity, the Glu3-Arg5 contact is highly populated in all variants invalidating it as a good indicator for comparing sequences. Overall, the contact map of Aβ40-VNL is similar to that of Aβ42-WT but with reduced propensities of SBs that make it difficult to justify that Aβ40-VNL oligomerization pathways are similar to those of Aβ42-WT.

III.VII. Importance of β-Turn and β-Hairpin at C-Terminus: Truncated Peptides. Because both Aβ40 and Aβ42 have a turn at residues 6−9 (Turn #1 (T1)), 14−16 (T2), and 23−27 (T3),[25] it is reasonable to hypothesize that these regions cannot alone contribute significantly to the difference in behavior of the two peptides. However, it was observed that there is a turn at 35−38 residues (T4) at the Aβ42 C-terminus with a significantly larger number of intramolecular contacts than that in Aβ40. More importantly, a β-hairpin with a β-turn at 36−37 positions occurs in Aβ42 but not in Aβ40. To confirm this experimental observation, the REMD simulation was performed for the truncated peptides Aβ_{31-40} and Aβ_{31-42}, and their mutants using the PARM99SB force field and implicit solvent.[25] For comparison, we also carried out the implicit solvent all-atom REMD, but with the OPLS-AA/L force field.[32] The initial structures of truncated peptides were obtained from the initial structures of the full-length peptides removing unnecessary fragments. The temperatures for replica exchange were chosen to be the same as for the full-length case (Section II). The duration of MD simulation was 500 ns, from which the first 100 ns were excluded as time for equilibrium and snapshots collected in the last 100−500 ns interval were used for data analysis.

As is evident from Table 5, the populations of β-turn obtained in our simulations are higher than the values reported by Teplow's group.[25] This is presumably due to not only the different force fields used in the simulations, but also the fact that we used all collected snapshots for estimating the turn content whereas they took into account only those from the most populated cluster.[25] Nevertheless, both simulations show that the VPV substitution dramatically levels up the β-turn propensity at the C-terminus of truncated peptides. The increase is about 46 and 36% for truncated Aβ42 and Aβ40, respectively, in our simulation whereas the corresponding values are 40 and 27% from the previous study.[25] Based on the high β-turn content of Aβ_{31-40}-VPV (35%) relative to Aβ_{31-42}-WT (25%), Teplow et al. hypothesized that upon VPV mutation, oligomerization pathways of full-length Aβ40-VPV become similar to those of Aβ-WT.

Table 5. Comparison of β-Turn and β-Hairpin Contents (%) of Truncated Peptides Aβ_{31-40} and Aβ_{31-42}, and VPV Mutants with the Results of Roychaudhuri et al.[25] (Boldface)[a]

sequences	β-hairpin	**β-hairpin[25]**	β-turn	**β-turn[25]**
Aβ_{31-42}-WT	28.6 ± 3.9	**5.5**	34.0 ± 3.9	**25**
Aβ_{31-42}-VPV	75.5 ± 3.3	**12.5**	80.4 ± 5.0	**65**
Aβ_{31-40}-WT	0.4 ± 0.7	**N/A**	10.3 ± 0.5	**8**
Aβ_{31-40}-VPV	15.9 ± 5.0	**N/A**	46.6 ± 5.0	**35**

[a]We used all collected snapshots in the data analysis whereas only conformations of the most populated cluster were previously taken into account.[25]

We found that the VPV mutation increases the β-hairpin content (see Figure 7 for representative structures of β-hairpin with turn at 36−37 positions) of Aβ_{31-42} from 28.6 to 75.5% (Table 5). The β-hairpin in our simulations is more abundant than in the simulations of Teplow et al.,[25] who reported 5.5 and 12.5% for Aβ_{31-42}-WT and Aβ_{31-42}-VPV, respectively. Again, the discrepancy is presumably due to different force fields and the ways of collecting data, as mentioned above. A hairpin does not appear in Aβ_{31-40}-WT (0.4%) but upon VPV substitution it occurs in about 16% of all collected snapshots.

Based on the high β-turn content of Aβ_{31-40}-VPV (35%) relative to that of Aβ_{31-42}-WT (25%), Roychaudhuri et al. hypothesized that upon VPV mutation, oligomerization pathways of full-length Aβ40-VPV become similar to the Aβ-WT ones. As is evident from our simulations, the β-turn propensity of Aβ_{31-40}-VPV (46.6%) is also higher than that of Aβ_{31-42}-WT supporting this experimental fact[25] but, as shown below, this is not valid for the full-length case.

III.VIII. β-Turn and β-Hairpin at C-Terminus: Full-Length Peptides. Because the behavior of full-length peptides may be different from that of truncated ones, we carried out all-atom REMD simulations for Aβ40 and Aβ42, and their variants with VPV mutation. The importance of triple mutations at positions 33, 36, and 38 was further tested through a study of the impact of a new mutation Gly33Val-Val36Asn-Gly38Leu (VNL) on β-turn and β-hairpin contents at the C-terminus.

In our simulations, the β-turn content of Aβ40-WT and Aβ42-WT is higher than that of their truncated fragments Aβ_{31-40}-WT and Aβ_{31-42}-WT (Tables 5 and 6). Upon VPV

DOI: 10.1021/acs.jpcb.6b12888
J. Phys. Chem. B 2017, 121, 4341−4354

Table 6. Occupancy of β-Turn at Residues 36, 37, and β-Hairpin at C-Terminal of Full-Length Aβ and Their Mutants[a]

sequences	β-turn (%)	β-hairpin (%)
Aβ42-WT	42.9 ± 1.5	14.0 ± 1.8
Aβ42-VPV	53.8 ± 2.4	32.0 ± 3.5
Aβ42-VNL	53.9 ± 4.0	32.0 ± 5.0
Aβ40-WT	13.3 ± 0.6	0.1 ± 0.3
Aβ40-VPV	19.4 ± 1.4	0.0 ± 0.1
Aβ40-VNL	16.7 ± 1.2	0.5 ± 0.5

[a]Results were obtained at equilibrium.

mutation, it drops from 80.4 for Aβ_{31-42}-VPV to 53.8% for Aβ42-VPV, whereas it is 46.6 and 19.4% for Aβ_{31-40}-VPV and Aβ40-VPV, respectively. Thus, the size effect is distinct for the WT and mutations. It should be noted that the difference between full-length and truncated variants comes from the cross-talk between regions 1−16 and 17−42, as is evident from the nonzero populations of SBs Arg5-Glu22, Arg5-Asp23, and in some cases of Asp7-Lys28 (Figure 9).

The propensity of β-turn of Aβ40-WT (13.3%) is lower than that of Aβ42-WT (42.9%). There is almost no β-hairpin centered at V36−G37 in Aβ40 (0.1%) but its occupancy is 14% in Aβ42 (Table 4). The pronounced difference in the C-terminal β-turn and β-hairpin results in distinct aggregation pathways and rates of Aβ40 and Aβ42.

The VPV mutation levels up the population of the β-turn and β-hairpin of Aβ42 from 42.9 to 53.8% and 14 to 32%, respectively (Table 4). The increase of these quantities is in line with the experimental work[25] showing that the stability of β-hairpin is enhanced because Aβ42-VPV displayed a high β-content immediately after dissolution, whereas Aβ42-WT existed in SC form after 5 days of incubation. The results of ThT fluorescence also matches these observations. Thus, the increased β-hairpin content, relative to that found in Aβ42-WT, implies that the Aβ42-VPV β-sheet structure is more stable. More importantly, the enhanced β-turn and β-hairpin contents of Aβ42-VPV compared to those of Aβ42-WT are consistent with the experimental fact that these variants oligomerize in distinct pathways resulting in different oligomer distributions.[25] Namely, the method of photo-induced cross-linking of unmodified proteins showed that Aβ42 displayed monomer and trimer bands whereas monomer, pentamer, and hexamer were observed for Aβ42-VPV.

For Aβ40, VPV increases β-turn propensity from 13.3 to 19.4% but leaves the β-hairpin population unchanged (about 0%). This was not surprising considering the decreased number of HB donors/acceptors and the decreased hydrophobic interaction potential at the C-terminus of the Aβ40 compared with that of the Aβ42 peptides (Figure 7). Only three residues exist after the turn in the Aβ40 system, as opposed to five in the Aβ42 system, meaning that although the VPV substitution enables formation of a turn, the overall stability is lower due to the lack of the other two amino acids. Our result matches that of Roychaudhuri et al., whereby Aβ40-VPV produces a poor β-hairpin structure, though the β-turn was observed for residues 35−38.[25]

Assuming that oligomerization pathways depend on the existence of a β-turn and β-hairpin at the C-terminus,[25] it is difficult to argue that the VPV mutation makes the behavior of Aβ40 similar to that of Aβ42 because the propensity of the β-turn and β-hairpin of Aβ40-VPV is much lower than that of Aβ42-WT (19.4 and 0% against 42.9 and 14%, Table 6). In contrast, based on the substantial increase of β-turn in the truncated fragment Aβ_{31-40} due to VPV mutation (25% for Aβ_{31-42}-WT and 35% for Aβ_{31-40}-VPV, Table 5), it has been proposed that the oligomerization pathways of full-length Aβ40-VPV and Aβ42-WT are similar.[25] Thus, the prediction based on simulations of short fragments is different to that obtained from study of the full-length peptides. In our opinion, to explain why Aβ40-VPV and Aβ42-WT oligomerize similarly, one has to consider not only the C-terminal β-turn content but also the β-structure of the whole sequence. Having nearly the same β-structures (Tables 1 and 2), these sequences are expected to have similar aggregation rates and pathways.

The VNL mutation levels up the population of β-turn and β-hairpin at the C-terminal of Aβ42 to the same extent that VPV does (Table 6) confirming that VNL has the same effect as the VPV mutation of enhancing the hydrophobic interaction in two β strands at the C-terminal. Roychaudhuri et al.[25] showed that Aβ42-VPV is more toxic than Aβ42-WT, suggesting that Aβ42-VNL, which has the same motif of C-terminal structure as that of Aβ42-VPV, is also expected to be more toxic than the Aβ42-WT. In other words, upon VNL mutation, Aβ42 becomes super-Aβ42.

The VNL mutation increases the β-turn propensity of Aβ40 from 13.3 to 16.7% but does not change the β-hairpin population (about 0%) at the C-end. So, the β-turn and β-hairpin contents of Aβ40-VNL and Aβ40-VPV are nearly the same and we expect that the oligomerization pathways of these sequences will be similar to those of Aβ42-WT, but mainly due to the mutation-induced enhancement of the β-structure (Tables 1 and 2).

III.IX. Robustness of Our Results against Force Fields.

The reliability of various combinations of different Amber force fields and implicit water models has been probed,[71−73] but none of them has pronounced advantages over each other. To test the robustness of the OPLS results, we additionally performed the REMD simulation using the force field Amber96[74] and OBC water model[33] (now referred to as ff96-OBC). The rationale for our choice was not only that the ff96-OBC combination was available in the Gromacs software, but also because it is capable of distinguishing structured from unstructured conformations and predicting a β-hairpin when appropriate.[73]

For the REMD simulation with 500 ns per replica we used the same temperature interval as in the OPLS case. Monitoring the time dependence of RMSD, one can show that all studied systems involving Aβ40-WT, Aβ40-VPV, Aβ42-WT, and Aβ42-VPV reached equilibrium at about 210 ns (results not shown).

III.IX.I. Secondary Structures of the Whole Sequences. Using structures sampled in the last 290 ns, we estimated the secondary structures shown in Table S4. ff96-OBC gives a much higher β-content compared to that from OPLS (Tables 1 and 2) and other simulation estimates.[26,29,64,65] However, for Aβ40-WT, the β-structure of 27% is compatible with 25% reported by Rosenman et al.,[55] and for Aβ42-WT, our value of 49% is not far from the value of 56% from Mitternacht et al.[68] Although the β-sheet is highly populated in ff96-OBC, this model captures the main fact that Aβ42-WT is more ordered than Aβ40-WT. More importantly, upon VPV mutation the β-structure levels up from 27 to 54% (Table S4), which is close to 49% of Aβ42-WT. The turn and coil populations of Aβ40-VPV are also nearly equal to those of Aβ42-WT. In addition, the per-residue distributions of β-content of these two sequences are

DOI: 10.1021/acs.jpcb.6b12888
J. Phys. Chem. B 2017, 121, 4341−4354

similar such that the most populated residues (>50%) are 2−4, 10−14, 18−23, and 31−37 for Aβ40-VPV, and for Aβ42-WT, they are 2−5, 9−13, 18−23, 30−35, and 38−41 (Figures S1 and S2). Taken together, similar to OPLS, ff96-OBC mimics the key experimental fact[25] that in terms of aggregation properties, the mutation VPV makes Aβ40 behave like Aβ42. With the VPV mutation, a slight increase in β-content was seen in both OPLS and ff96-OBC (Tables 2 and S2).

III.IX.II. Population of β-Turn and Hairpin at C-Terminus. As in the OPLS case, the VPV mutation only slightly levels up the populations of β-turn at residues 36 and 37, and of the short hairpin at the C-terminal of Aβ40 such that they still remain far below those of Aβ42-WT (cf. Tables 6 and S5). In other words, such an effect is not strong enough to change the aggregation kinetics of Aβ40. Therefore, together with OPLS the ff90-OBC combination supports our main hypothesis that the promotion of β-content of the whole sequence is the main factor in converting the Aβ40 behavior into Aβ42 behavior upon VPV mutation. We anticipate that this conclusion remains valid in other force fields.

Similar to the OPLS case for Aβ42, the VPV mutation significantly increases the β-turn from 42.3 to 72.6%, and the occupancy of hairpin, centered at 36−37 residues, jumps from 29.8 to 60.7%. This result is in the line with the experimental fact that the VPV mutation produced super-Aβ42.[25] Thus, both force fields can capture the superior behavior of Aβ42-VPV.

IV. CONCLUSIONS

By REMD simulation with the OPLS-AA/L force field[32] in implicit solvent, we have clarified the influence of the VPV and VNL mutations on the structures of Aβ40 and Aβ42. In agreement with recent experiments,[25] we showed that Aβ42-WT is richer in β-turn at the C-terminus than that of Aβ40-WT. Furthermore, a short β-hairpin centered at 36−37 residues occurs in Aβ42 but not in Aβ40. VPV and VNL mutations promote the β-structure in both Aβ40 and Aβ42, in particular, making the C-terminal of Aβ40 mutants more ordered than that of its WT. The β-turn content at this end is more populated but the mutations fail to promote formation of a β-hairpin, as in the Aβ42 case, due to the lack of the last two residues. However, present and previous[25] simulations show that a short β-hairpin is populated in the truncated $A\beta_{31-40}$-VPV with a considerable amount of β-turn at the C-terminal. Based on this fact, Roychaudhuri et al.[25] hypothesized that oligomerization pathways of Aβ40-VPV are similar to those of Aβ42-WT due to the high content of β-turn. In contrast, our simulations for full-length peptides show that although VPV mutation promotes β-turn at the C-terminal of Aβ40, it remains noticeably lower than that of Aβ42-WT. In addition, a short β-hairpin centered at 36−37 positions is present in Aβ42-WT but not in Aβ40-VPV. All of this evidence led us to the suggestion that similar aggregation pathways of Aβ40-VPV and Aβ42-WT, revealed by experimental data on oligomer distributions, were caused not only by the presence of β-turn and hairpin at the C-terminal (Table 6) but also by increased β-content over the whole sequence upon mutation (Tables 1 and 2).

We have shown that the cross-talk between charged residues in the N- and C-terminal is behind the distinct contents of β-turn and β-hairpin at the C-terminal of full-length and truncated peptides. Therefore, one of our main findings is that predictions for the full-length case based on results obtained for truncated variants may be misleading.

For Aβ42, VPV and VNL produce super-Aβ42 enhancing the β-ordering, and in particular, the stability of the C-terminal. Because Aβ42-VPV is more toxic than WT,[25] and both mutants have the same β-turn and β-hairpin contents at the C-terminal (Table 6), one can expect that Aβ42-VNL is also more toxic than Aβ42-WT. It would be very interesting to check this prediction, as well as the similarity in self-aggregation pathways of Aβ40-VNL and Aβ42-WT by in vitro experiments.

Because the hydrophobicity of Gly, Val, Pro, Leu, and Asn is −0.4, 4,2, −1.6, 3.8, and −3.5, mutations VPV and VNL level up the total hydrophobicity by 3.4 and 1.1, respectively. Thus, the enhancement of Aβ stability or of the fibril-prone state propensity is ultimately due to an increase in hydrophobicity, which is consistent with general principles governing fibril formation.[57] The new observation here is that the hydrophobicity enhancement due to mutations at positions 33, 36, and 38 promote β-hairpin and β-turn centered at 36−37 residues not only in truncated fragments[25] but also in full-length peptides, as shown for the first time in this work. To further cement this point of view, in addition to VNL, we also carried out simulations for the Gly33Val-Val36Asp-Gly38Leu (VDL) mutation, which increases hydrophobicity by 1.1, as in the VNL case. The obtained results (not shown) fully support the important role of enhanced hydrophobicity in stabilizing the β-turn and hairpin structure at the C-terminus. The role of the charged residue Asp36 seems to be minor compared to the hydrophobic effect.

The robustness of our results against theoretical models was probed by performing additional simulations with the Amber96 force field in combination with implicit OBC water model. We have shown that although in ff96-OBC, the Aβ monomers become more ordered than those in OPLS, the increase in β-content of Aβ40 upon VPV mutation is a key factor in converting the Aβ40 behavior into Aβ42 behavior because the change in population of the β-turn and hairpin at the C-terminus is minor. In the Aβ42 case, both force fields ascertain that the increased population of the β-turn and hairpin leads to the super behavior of Aβ42-VPV. Thus, our main results are supported by two force fields with different implicit water models. As mentioned above, because water bridges play a minor role in the stability of intrinsically disordered Aβ, the application of all-atom models with explicit water presumably will not change the major conclusions. However, this interesting problem is left for future study.

■ ASSOCIATED CONTENT

Supporting Information

The Supporting Information is available free of charge on the ACS Publications website at DOI: 10.1021/acs.jpcb.6b12888.

Populations of SB, Asp23-Lys28 HB or SB for full-length Aβ variants; REMD simulation with Amber96 and OBC water model; per-residue distributions of secondary structures of Aβ40-WT and Aβ40-VPV; occupancy (%) of the β-turn and β-hairpin of full-length Aβ and their mutants (PDF)

■ AUTHOR INFORMATION

Corresponding Author

*E-mail: masli@ifpan.edu.pl. Phone: +48 22 843 66 01.

ORCID

Mai Suan Li: 0000-0001-7021-7916

DOI: 10.1021/acs.jpcb.6b12888
J. Phys. Chem. B 2017, 121, 4341−4354

Author Contributions

[▽]N.H.L. and T.T.M.T. contributed equally.

Author Contributions

M.S.L. conceived the experiments. N.H.L. and T.T.M.T. conducted the experiments. N.H.L., T.T.M.T., and M.S.L. analyzed the results. T.T.M.T., N.H.L., and M.S.L. wrote the paper. All authors reviewed the manuscript.

Funding

This work was supported by Department of Science and Technology at Ho Chi Minh City, Vietnam, and the Polish NCN grant 2015/19/B/ST4/02721, Poland. Allocation of CPU time at the supercomputer center TASK in Gdansk (Poland) is highly appreciated.

Notes

The authors declare no competing financial interest.

REFERENCES

(1) Greene, J. D.; Baddeley, A. D.; Hodges, J. R. Analysis of the Episodic Memory Deficit in Early Alzheimer's Disease: Evidence from the Doors and People Test. *Neuropsychologia* **1996**, *34*, 537−551.

(2) Price, B. H.; Gurvit, H.; Weintraub, S.; Geula, C.; Leimkuhler, E.; Mesulam, M. Neuropsychological Patterns and Language Deficits in 20 Consecutive Cases of Autopsy-Confirmed Alzheimer's Disease. *Arch. Neurol.* **1993**, *50*, 931−937.

(3) Esteban-Santillan, C.; Praditsuwan, R.; Veda, H.; Geldmacher, D. S. Clock Drawing Test in Very Mild Alzheimer's Disease. *J. Am. Geriatr. Soc.* **1998**, *46*, 1266−1269.

(4) Hardy, J.; Selkoe, D. J. The Amyloid Hypothesis of Alzheimer's Disease: Progress and Problems on the Road to Therapeutics. *Science* **2002**, *297*, 353−356.

(5) Alonso, A. d. C.; Zaidi, T.; Novak, M.; Grundke-Iqbal, I.; Iqbal, K. Hyperphosphorylation Induces Self-Assembly of T into Tangles of Paired Helical Filaments/Straight Filaments. *Proc. Natl. Acad. Sci. U.S.A.* **2001**, *98*, 6923−6928.

(6) Citron, M. Strategies for Disease Modification in Alzheimer's Disease. *Nat. Rev. Neurosci.* **2004**, *5*, 677−685.

(7) ACS chemical neuroscience Aguzzi, A.; O'Connor, T. Protein Aggregation Diseases: Pathogenicity and Therapeutic Perspectives. *Nat. Rev. Drug Discovery* **2010**, *9*, 237−248.

(8) Eanes, E. D.; Glenner, G. X-Ray Diffraction Studies on Amyloid Filaments. *J. Histochem. Cytochem.* **1968**, *16*, 673−677.

(9) Petkova, A. T.; Ishii, Y.; Balbach, J. J.; Antzutkin, O. N.; Leapman, R. D.; Delaglio, F.; Tycko, R. A Structural Model for Alzheimer's Beta -Amyloid Fibrils Based on Experimental Constraints from Solid State NMR. *Proc. Natl. Acad. Sci. U.S.A.* **2002**, *99*, 16742−16747.

(10) Lührs, T.; Ritter, C.; Adrian, M.; Riek-Loher, D.; Bohrmann, B.; Döbeli, H.; Schubert, D.; Riek, R. 3d Structure of Alzheimer's Amyloid-B (1−42) Fibrils. *Proc. Natl. Acad. Sci. U.S.A.* **2005**, *102*, 17342−17347.

(11) Nasica-Labouze, J.; Nguyen, P. H.; Sterpone, F.; Berthoumieu, O.; Buchete, N. V.; Cote, S.; De Simone, A.; Doig, A. J.; Faller, P.; Garcia, A.; et al. Amyloid Beta Protein and Alzheimer's Disease: When Computer Simulations Complement Experimental Studies. *Chem. Rev.* **2015**, *115*, 3518−3563.

(12) Gravina, S. A.; Ho, L.; Eckman, C. B.; Long, K. E.; Otvos, L.; Younkin, L. H.; Suzuki, N.; Younkin, S. G. Amyloid B Protein (A*β*) in Alzheimer's Disease Brain Biochemical and Immunocytochemical Analysis with Antibodies Specific for Forms Ending at A*β*40 or A*β*42 (43). *J. Biol. Chem.* **1995**, *270*, 7013−7016.

(13) Iwatsubo, T.; Odaka, A.; Suzuki, N.; Mizusawa, H.; Nukina, N.; Ihara, Y. Visualization of A*β*42 (43) and A*β*40 in Senile Plaques with End-Specific A*β* Monoclonals: Evidence That an Initially Deposited Species Is A*β*42 (43). *Neuron* **1994**, *13*, 45−53.

(14) Suzuki, N.; Cheung, T. T.; Cai, X. D.; Odaka, A.; Otvos, L.; Eckman, C.; Golde, T. E.; Younkin, S. G. An Increased Percentage of Long Amyloid Beta Protein Secreted by Familial Amyloid Beta Protein Precursor (Beta App717) Mutants. *Science* **1994**, *264*, 1336−1340.

(15) Golde, T. E.; Eckman, C. B.; Younkin, S. G. Biochemical Detection of A*β* Isoforms: Implications for Pathogenesis, Diagnosis, and Treatment of Alzheimer's Disease. *Biochim. Biophys. Acta, Mol. Basis Dis.* **2000**, *1502*, 172−187.

(16) Scheuner, D.; Eckman, C.; Jensen, M.; Song, X.; Citron, M.; Suzuki, N.; Bird, T.; Hardy, J.; Hutton, M.; Kukull, W.; et al. Secreted Amyloid Beta-Protein Similar to That in the Senile Plaques of Alzheimer's Disease Is Increased in Vivo by the Presenilin 1 and 2 and App Mutations Linked to Familial Alzheimer's Disease. *Nat. Med.* **1996**, *2*, 864−870.

(17) Lomakin, A.; Teplow, D. B.; Benedek, G. B. In *Amyloid Proteins: Methods and Protocols*; Sigurdsson, E. M., Calero, M., Gasset, M., Eds.; Springer Science & Business Media, 2005; Vol. *299*, pp 153−174.

(18) Lomakin, A.; Chung, D. S.; Benedek, G. B.; Kirschner, D. A.; Teplow, D. B. On the Nucleation and Growth of Amyloid Beta-Protein Fibrils: Detection of Nuclei and Quantitation of Rate Constants. *Proc. Natl. Acad. Sci.* **1996**, *93*, 1125−1129.

(19) Bernstein, S. L.; Dupuis, N. F.; Lazo, N. D.; Wyttenbach, T.; Condron, M. M.; Bitan, G.; Teplow, D. B.; Shea, J.-E.; Ruotolo, B. T.; Robinson, C. V. Amyloid-B Protein Oligomerization and the Importance of Tetramers and Dodecamers in the Aetiology of Alzheimer's Disease. *Nat. Chem.* **2009**, *1*, 326−331.

(20) Bitan, G.; Vollers, S. S.; Teplow, D. B. Elucidation of Primary Structure Elements Controlling Early Amyloid B-Protein Oligomerization. *J. Biol. Chem.* **2003**, *278*, 34882−34889.

(21) Lue, L.-F.; Kuo, Y.-M.; Roher, A. E.; Brachova, L.; Shen, Y.; Sue, L.; Beach, T.; Kurth, J. H.; Rydel, R. E.; Rogers, J. Soluble Amyloid B Peptide Concentration as a Predictor of Synaptic Change in Alzheimer's Disease. *Am. J. Pathol.* **1999**, *155*, 853−862.

(22) Bitan, G.; Kirkitadze, M. D.; Lomakin, A.; Vollers, S. S.; Benedek, G. B.; Teplow, D. B. Amyloid B-Protein (A*β*) Assembly: A*β*40 and A*β*42 Oligomerize through Distinct Pathways. *Proc. Natl. Acad. Sci. U.S.A.* **2003**, *100*, 330−335.

(23) Viet, M. H.; Nguyen, P. H.; Derreumaux, P.; Li, M. S. Effect of the English Familial Disease Mutation (H6r) on the Monomers and Dimers of A*β*40 and A*β*42. *ACS Chem. Neurosci.* **2014**, *5*, 646−657.

(24) Truong, P. M.; Viet, M. H.; Nguyen, P. H.; Hu, C.-K.; Li, M. S. Effect of Taiwan Mutation (D7h) on Structures of Amyloid-B Peptides: Replica Exchange Molecular Dynamics Study. *J. Phys. Chem. B* **2014**, *118*, 8972−8981.

(25) Roychaudhuri, R.; Yang, M.; Deshpande, A.; Cole, G. M.; Frautschy, S.; Lomakin, A.; Benedek, G. B.; Teplow, D. B. C-Terminal Turn Stability Determines Assembly Differences between A*β*40 and A*β*42. *J. Mol. Biol.* **2013**, *425*, 292−308.

(26) Sgourakis, N. G.; Yan, Y.; McCallum, S. A.; Wang, C.; Garcia, A. E. The Alzheimer's Peptides A*β*40 and 42 Adopt Distinct Conformations in Water: A Combined MD/NMR Study. *J. Mol. Biol.* **2007**, *368*, 1448−1457.

(27) Hou, L.; Shao, H.; Zhang, Y.; Li, H.; Menon, N. K.; Neuhaus, E. B.; Brewer, J. M.; Byeon, I.-J. L.; Ray, D. G.; Vitek, M. P.; et al. Solution NMR Studies of the A*β* (1−40) and A*β* (1−42) Peptides Establish That the Met35 Oxidation State Affects the Mechanism of Amyloid Formation. *J. Am. Chem. Soc.* **2004**, *126*, 1992−2005.

(28) Yan, Y.; Wang, C. A*β*42 Is More Rigid Than A*β*40 at the C Terminus: Implications for A*β* Aggregation and Toxicity. *J. Mol. Biol.* **2006**, *364*, 853−862.

(29) Yang, M.; Teplow, D. B. Amyloid B-Protein Monomer Folding: Free-Energy Surfaces Reveal Alloform-Specific Differences. *J. Mol. Biol.* **2008**, *384*, 450−464.

(30) Teplow, D. B.; Lazo, N. D.; Bitan, G.; Bernstein, S.; Wyttenbach, T.; Bowers, M. T.; Baumketner, A.; Shea, J.-E.; Urbanc, B.; Cruz, L. Elucidating Amyloid B-Protein Folding and Assembly: A Multidisciplinary Approach. *Acc. Chem. Res.* **2006**, *39*, 635−645.

(31) Lazo, N. D.; Grant, M. A.; Condron, M. C.; Rigby, A. C.; Teplow, D. B. On the Nucleation of Amyloid B-Protein Monomer Folding. *Protein Sci.* **2005**, *14*, 1581−1596.

(32) Kaminski, G. A.; Friesner, R. A.; Tirado-Rives, J.; Jorgensen, W. L. Evaluation and Reparametrization of the OPLS-AA Force Field for

DOI: 10.1021/acs.jpcb.6b12888
J. Phys. Chem. B 2017, 121, 4341−4354

Proteins Via Comparison with Accurate Quantum Chemical Calculations on Peptides. *J. Phys. Chem. B* **2001**, *105*, 6474−6487.
(33) Onufriev, A.; Bashford, D.; Case, D. A. Exploring Protein Native States and Large-Scale Conformational Changes with a Modified Generalized Born Model. *Proteins: Struct., Funct., Bioinf.* **2004**, *55*, 383−394.
(34) Hess, B.; Kutzner, C.; Van Der Spoel, D.; Lindahl, E. Gromacs 4: Algorithms for Highly Efficient, Load-Balanced, and Scalable Molecular Simulation. *J. Chem. Theory Comput.* **2008**, *4*, 435−447.
(35) Nguyen, P. H.; Li, M. S.; Derreumaux, P. Effects of All-Atom Force Fields on Amyloid Oligomerization: Replica Exchange Molecular Dynamics Simulations of the Aβ 16−22 Dimer and Trimer. *Phys. Chem. Chem. Phys.* **2011**, *13*, 9778−9788.
(36) Smith, M. D.; Rao, J. S.; Segelken, E.; Cruz, L. Force-Field Induced Bias in the Structure of a Beta(21−30): A Comparison of OPLS, Amber, Charmm, and Gromos Force Fields. *J. Chem. Inf. Model.* **2015**, *55*, 2587−2595.
(37) Nguyen, H. L.; Thu, T. T. M.; Truong, P. M.; Lang, P. D.; Man, V. H.; Nguyen, P. H.; Tu, L. A.; Chen, Y. C.; Li, M. S. A Beta 41 Aggregates More Like a Beta 40 Than Like a Beta 42: In Silico and in Vitro Study. *J. Phys. Chem. B* **2016**, *120*, 7371−7379.
(38) Yang, M. F.; Yordanov, B.; Levy, Y.; Bruschweiler, R.; Huo, S. H. The Sequence-Dependent Unfolding Pathway Plays a Critical Role in the Amyloidogenicity of Transthyretin. *Biochemistry* **2006**, *45*, 11992−12002.
(39) Lei, H.; Wu, C.; Liu, H. G.; Duan, Y. Folding Free-Energy Landscape of Villin Headpiece Subdomain from Molecular Dynamics Simulations. *Proc. Natl. Acad. Sci. U.S.A.* **2007**, *104*, 4925−4930.
(40) Hockney, R.; Goel, S.; Eastwood, J. Quiet High-Resolution Computer Models of a Plasma. *J. Comput. Phys.* **1974**, *14*, 148−158.
(41) Hess, B.; Bekker, H.; Berendsen, H. J.; Fraaije, J. G. LINCS: A Linear Constraint Solver for Molecular Simulations. *J. Comput. Chem.* **1997**, *18*, 1463−1472.
(42) Bussi, G.; Donadio, D.; Parrinello, M. Canonical Sampling through Velocity Rescaling. *J. Chem. Phys.* **2007**, *126*, No. 014101.
(43) Patriksson, A.; van der Spoel, D. A Temperature Predictor for Parallel Tempering Simulations. *Phys. Chem. Chem. Phys.* **2008**, *10*, 2073−2077.
(44) Frishman, D.; Argos, P. Knowledge-Based Protein Secondary Structure Assignment. *Proteins: Struct., Funct., Bioinf.* **1995**, *23*, 566−579.
(45) Heinig, M.; Frishman, D. Stride: A Web Server for Secondary Structure Assignment from Known Atomic Coordinates of Proteins. *Nucleic Acids Res.* **2004**, *32*, W500−W502.
(46) Mu, Y.; Nguyen, P. H.; Stock, G. Energy Landscape of a Small Peptide Revealed by Dihedral Angle Principal Component Analysis. *Proteins: Struct., Funct., Bioinf.* **2005**, *58*, 45−52.
(47) Hutchinson, E. G.; Thornton, J. M. A Revised Set of Potentials for B-Turn Formation in Proteins. *Protein Sci.* **1994**, *3*, 2207−2216.
(48) Lewis, P. N.; Momany, F. A.; Scheraga, H. A. Chain Reversals in Proteins. *Biochim. Biophys. Acta* **1973**, *303*, 211−229.
(49) Richardson, J. S. The Anatomy and Taxonomy of Protein Structure. *Adv. Protein Chem.* **1981**, *34*, 167−339.
(50) Zhang, S.; Iwata, K.; Lachenmann, M.; Peng, J.; Li, S.; Stimson, E.; Lu, Y.-A.; Felix, A.; Maggio, J.; Lee, J. The Alzheimer's Peptide Aβ Adopts a Collapsed Coil Structure in Water. *J. Struct. Biol.* **2000**, *130*, 130−141.
(51) Danielsson, J.; Jarvet, J.; Damberg, P.; Gräslund, A. The Alzheimer B-Peptide Shows Temperature-Dependent Transitions between Left-Handed 31-Helix, B-Strand and Random Coil Secondary Structures. *FEBS J.* **2005**, *272*, 3938−3949.
(52) Kirkitadze, M. D.; Condron, M. M.; Teplow, D. B. Identification and Characterization of Key Kinetic Intermediates in Amyloid B-Protein Fibrillogenesis. *J. Mol. Biol.* **2001**, *312*, 1103−1119.
(53) Ono, K.; Condron, M. M.; Teplow, D. B. Structure−Neurotoxicity Relationships of Amyloid B-Protein Oligomers. *Proc. Natl. Acad. Sci. U.S.A.* **2009**, *106*, 14745−14750.
(54) Rojas, A.; Liwo, A.; Browne, D.; Scheraga, H. A. Mechanism of Fiber Assembly: Treatment of Aβ Peptide Aggregation with a Coarse-Grained United-Residue Force Field. *J. Mol. Biol.* **2010**, *404*, 537−552.
(55) Rosenman, D. J.; Connors, C. R.; Chen, W.; Wang, C.; García, A. E. Aβ Monomers Transiently Sample Oligomer and Fibril-Like Configurations: Ensemble Characterization Using a Combined Md/Nmr Approach. *J. Mol. Biol.* **2013**, *425*, 3338−3359.
(56) Meral, D.; Urbanc, B. Discrete Molecular Dynamics Study of Oligomer Formation by N-Terminally Truncated Amyloid B-Protein. *J. Mol. Biol.* **2013**, *425*, 2260−2275.
(57) Li, M. S.; Co, N. T.; Reddy, G.; Hu, C. K.; Straub, J. E.; Thirumalai, D. Factors Governing Fibrillogenesis of Polypeptide Chains Revealed by Lattice Models. *Phys. Rev. Lett.* **2010**, *105*, No. 218101.
(58) Lam, A.; Teplow, D.; Stanley, H.; Urbanc, B. Effects of the Arctic (E22 → G) Mutation on Amyloid B-Protein Folding: Discrete Molecular Dynamics Study. *J. Am. Chem. Soc.* **2008**, *130*, 17413−17422.
(59) Lin, Y.-S.; Pande, V. S. Effects of Familial Mutations on the Monomer Structure of Aβ 42. *Biophys. J.* **2012**, *103*, L47−L49.
(60) Snyder, S. W.; Ladror, U. S.; Wade, W. S.; Wang, G. T.; Barrett, L. W.; Matayoshi, E. D.; Huffaker, H. J.; Krafft, G. A.; Holzman, T. F. Amyloid-Beta Aggregation: Selective Inhibition of Aggregation in Mixtures of Amyloid with Different Chain Lengths. *Biophys. J.* **1994**, *67*, 1216−1228.
(61) Ball, K. A.; Phillips, A. H.; Wemmer, D. E.; Head-Gordon, T. Differences in B-Strand Populations of Monomeric Aβ40 and Aβ42. *Biophys. J.* **2013**, *104*, 2714−2724.
(62) Viet, M. H.; Li, M. S. Amyloid Peptide Aβ40 Inhibits Aggregation of Aβ42: Evidence from Molecular Dynamics Simulations. *J. Chem. Phys.* **2012**, *136*, No. 245105.
(63) Han, M.; Hansmann, U. H. Replica Exchange Molecular Dynamics of the Thermodynamics of Fibril Growth of Alzheimer's Aβ42 Peptide. *J. Chem. Phys.* **2011**, *135*, No. 065101.
(64) Côté, S.; Derreumaux, P.; Mousseau, N. Distinct Morphologies for Amyloid Beta Protein Monomer: Aβ1−40, Aβ1−42, and Aβ1−40 (D23n). *J. Chem. Theory Comput.* **2011**, *7*, 2584−2592.
(65) Velez-Vega, C.; Escobedo, F. A. Characterizing the Structural Behavior of Selected Aβ-42 Monomers with Different Solubilities. *J. Phys. Chem. B* **2011**, *115*, 4900−4910.
(66) Irbäck, A.; Mohanty, S. Folding Thermodynamics of Peptides. *Biophys. J.* **2005**, *88*, 1560−1569.
(67) Sgourakis, N. G.; Merced-Serrano, M.; Boutsidis, C.; Drineas, P.; Du, Z.; Wang, C.; Garcia, A. E. Atomic-Level Characterization of the Ensemble of the Aβ (1−42) Monomer in Water Using Unbiased Molecular Dynamics Simulations and Spectral Algorithms. *J. Mol. Biol.* **2011**, *405*, 570−583.
(68) Mitternacht, S.; Staneva, I.; Härd, T.; Irbäck, A. Comparing the Folding Free-Energy Landscapes of Aβ42 Variants with Different Aggregation Properties. *Proteins: Struct., Funct., Bioinf.* **2010**, *78*, 2600−2608.
(69) Sciarretta, K. L.; Gordon, D. J.; Petkova, A. T.; Tycko, R.; Meredith, S. C. Aβ40-Lactam (D23/K28) Models a Conformation Highly Favorable for Nucleation of Amyloid. *Biochemistry* **2005**, *44*, 6003−6014.
(70) Kumar, S.; Nussinov, R. Salt Bridge Stability in Monomeric Proteins. *J. Mol. Biol.* **1999**, *293*, 1241−1255.
(71) Shell, M. S.; Ritterson, R.; Dill, K. A. A Test on Peptide Stability of Amber Force Fields with Implicit Solvation. *J. Phys. Chem. B* **2008**, *112*, 6878−6886.
(72) Robinson, M. K.; Monroe, J. I.; Shell, M. S. Are Amber Force Fields and Implicit Solvation Models Additive? A Folding Study with a Balanced Peptide Test Set. *J. Chem. Theory Comput.* **2016**, *12*, 5631−5642.
(73) Maffucci, I.; Contini, A. An Updated Test of Amber Force Fields and Implicit Solvent Models in Predicting the Secondary Structure of Helical, Beta-Hairpin, and Intrinsically Disordered Peptides. *J. Chem. Theory Comput.* **2016**, *12*, 714−727.

DOI: 10.1021/acs.jpcb.6b12888
J. Phys. Chem. B 2017, 121, 4341−4354

(74) Kollman, P. A. Advances and Continuing Challenges in Achieving Realistic and Predictive Simulations of the Properties of Organic and Biological Molecules. *Acc. Chem. Res.* **1996**, *29*, 461−469.

DOI: 10.1021/acs.jpcb.6b12888
J. Phys. Chem. B 2017, 121, 4341−4354